Free-standing flexible and biomimetic hybrid membranes for ions and ATP transport

Molina, Brenda G; Lopes-Rodrigues, Maximilien; Estrany, Francesc; Michaux, Catherine; Perpete, Eric A; Armelin, Elaine; Aleman, Carlos

Published in:
Journal of Membrane Science

DOI:
10.1016/j.memsci.2020.117931

Publication date:
2020

Journal of Membrane Science 601 (2020) 117931

Contents lists available at ScienceDirect

Journal of Membrane Science

journal homepage: http://www.elsevier.com/locate/memsci

Free-standing flexible and biomimetic hybrid membranes for ions and ATP transport

Brenda G. Molina [a,c], Maximilien Lopes-Rodrigues [a,b], Francesc Estrany [a,c], Catherine Michaux [b], Eric A. Perpète [b], Elaine Armelin [a,b], Carlos Alemán [a,c,d,*]

[a] Departament d'Enginyeria Química and Barcelona Research Center for Multiscale Science and Engineering, EEBE, Universitat Politècnica de Catalunya, C/Eduard Maristany 10-14, Edif. I, 08019, Barcelona, Spain

[b] Laboratoire de Chimie Physique des Biomolécules, Unité de Chimie Physique Théorique et Structurale (UCPTS), University of Namur, Rue de Bruxelles, 61, 5000, Namur, Belgium

[c] Barcelona Research Center for Multiscale Science and Engineering, EEBE, Universitat Politècnica de Catalunya, C/Eduard Maristany 10-14, Edif. C, 08019, Barcelona, Spain

[d] Institute for Bioengineering of Catalonia (IBEC), The Barcelona Institute of Science and Technology, Baldiri Reixac 10-12, 08028, Barcelona, Spain

ARTICLE INFO

Keywords:
Conducting polymers
Membranes
Polylactic acid
Membrane proteins
Self-supported films

ABSTRACT

The transport of metabolites across robust, flexible and free-standing biomimetic membranes made of three perforated poly (lactic acid) (pPLA) layers, separated by two anodically polymerized conducting layers of poly (3,4-ethylenedioxythiophene-*co*-3-dodecylthiophene), and functionalized on the external pPLA layers with a voltage dependent anion channel (VDAC) protein, has been demonstrated. The three pPLA layers offer robustness and flexibility to the bioactive platform and the possibility of obtaining conducing polymer layers by *in situ* anodic polymerization. The incorporation of dodecylthiophene units, which bear a 12 carbon atoms long linear alkyl chain, to the conducting layers allows mimicking the amphiphilic environment offered by lipids in cells, increasing 32% the efficiency of the functionalization. Electrochemical impedance measurements in NaCl and adenosine triphosphate (ATP) solutions prove that the integration of the VDAC porin inside the PLA perforations considerably increases the membrane conductivity and is crucial for the electrolyte diffusion. Such results open the door for the development of advanced sensing devices for a broad panel of biomedical applications.

1. Introduction

Biomimetics takes advantage of the natural structures found in biological systems, permitting a nanoscopic development of functional materials. Within this context, nanomaterials based on proteins offer countless potential nano-sized devices such as nanoreactors [1], filtration devices [2], nanosensors [3,4], or drug delivery systems [5]. Many of these applications usually require channel shaped components, which provide nanoscopic pathways for the passage of ions and small molecules. Appropriately, a class of outer membrane proteins (OMPs) found in *gram*-negative bacteria and mitochondria, called porins, can naturally form β-barrel channels [6]. They act as gates of the cell membrane. The majority of the porins does not present any particular selectivity and allows the passive diffusion of hydrophilic solutes (*e.g.* ions, sugars, amino acids and ATP) [7].

The outside facing part of β-barrel channels is hydrophobic to match the alkyl chains of the membrance lipids, while the internal water-filled part contains charged and hydrophilic residues. The size of the pore, which usually ranges from 10 to 40 Å, prevents bulky molecules to be diffused and the internal hydrophilic region defines the permeation mechanism of species crossing the channel [8]. In addition, β-barrels exhibit exceptional robustness and stability over time and temperature [9,10]. Those features make porins competitive for their insertion in non-biological synthetic environment such as polymers. From such perspective, the approaches used to modify polymeric membranes, which can be free-standing or tethered onto solid supports, with functional biomolecules are based on the utilization of amphiphilic copolymers and structured polymers [3].

In a recent study, ion-responsive hybrid nanomembranes (NMs) were developed by combining poly (*N*-methylpyrrole) (PNMPy), a conducting

* Corresponding author. Departament d'Enginyeria Química and Barcelona Research Center for Multiscale Science and Engineering, EEBE, Universitat Politècnica de Catalunya, C/Eduard Maristany 10-14, Edif. I, 08019, Barcelona, Spain.
E-mail address: carlos.aleman@upc.edu (C. Alemán).

https://doi.org/10.1016/j.memsci.2020.117931
Received 19 September 2019; Received in revised form 2 February 2020; Accepted 4 February 2020
Available online 5 February 2020

polymer (CP) that was electrochemically synthesized onto a rigid stainless steel electrode, with the Omp2a porin [11]. Electrochemical studies on the resulting system (PNMPy/Omp2a) showed the activity of the protein to promote the passive transport of K^+ through the CP membrane. More recently, another hybrid NM was engineered by immobilizing the same protein onto nanoperforated poly (lactic acid) (npPLA) NMs, the resulting system being denoted npPLA/Omp2a [12]. Immobilization of the protein around and inside the nanoperforations, which exhibited an average diameter of 51 ± 22 nm and a depth of ~100 nm, greatly increased the material conductivity and selectivity against some ions. Despite the capacity of npPLA and npPLA/Omp2a NMs to be free-standing, the difficulties associated with their handling limited ion diffusion and electrical measurements, which were conducted using NMs supported onto ITO substrates [12]. Under these conditions, the conductivity of npPLA/Omp2a membranes was comparable to that of the same protein supported onto lipid bilayers (LB/Omp2a) [13]. However, the suppression of the solid support to have biomimetic and flexible platforms with conducting channels for the metabolite transport is highly desirable.

Taking advantages of previous studies based on PNMPy/Omp2a, npPLA/Omp2a and LB/Omp2a [11–13], the novelty of the present work relies on the design of an advanced functional platform by immobilizing porin proteins onto a smart free-standing biomimetic membrane. This biomimetic membrane consists of three PLA layers with sub-micrometric perforations (pPLA layers) separated by two layers of a CP, which was prepared by electropolymerization. Although poly (3, 4-ethylenedioxythiophene) (PEDOT) is the most stable and electroactive heterocyclic CP [14–18], in this work the two conducting layers have been prepared using a copolymer (COP) of 3,4-ethylenedioxythiophene (EDOT; Scheme 1a) and 3-dodecylthiophene (3DT; Scheme 1b). The incorporation of 3DT units, which bears a 12 carbon atoms long linear alkyl chain, is aimed to mimic the natural amphiphilic environment required by OMPs (*i.e.* like that offered by lipids), without the losing the excellent conducting properties of PEDOT.

The resulting free-standing 5-layered membrane, hereafter named 5-pPLA/COP, has been transformed into 5-pPLA/COP/VDAC by immobilizing a Voltage Dependent Anion Channel (VDAC) protein (Scheme 1c) at the external pPLA layers. VDACs are porins found in the outer mitochondrial membrane of all eukaryotic cells, which are associated with the permeability of the mitochondria [19] and regulate the diffusion of ions and metabolites, such as nicotinamide adenine dinucleotide hydrogen (NADH) or adenosine triphosphate (ATP) [20]. The protein used to prepare 5-pPLA/COP/VDAC is VDAC36 from *Solanum tuberosum*, a plant model organism [21]. Although the molecular weight of this voltage-dependent anion selective porin is similar to that of Omp2a (36 and 39 kDa, respectively), these two proteins highly differ in the diameter of their channels. The effective diameter of the protein channel of VDAC36 and Omp2a is about 2.0 and 1.2 nm, respectively, and, therefore, the former is expected to allow the diffusion of larger solutes than the latter [22,23]. In order to ascertain the influence of the dodecyl side groups in the functionalized device, the performance of 5-pPLA/-COP/VDAC and 5-pPLA/PEDOT/VDAC (Scheme 1c), in which the two COP layers have been substituted by the PEDOT homopolymer, has been compared. Moreover, the benefits provided by the VDAC36 protein have been evaluated by comparing the transport of ions across protein functionalized and non-functionalized free-standing membranes, the latter being named 5-pPLA/COP and 5-pPLA/PEDOT.

2. Materials and methods

2.1. Materials

PEDOT:poly (styrene sulfonate) (PSS) 1.3 wt % dispersion in water, EDOT and 3DT monomers, poly (vinyl alcohol) (PVA) 87–89% hydrolyzed and lithium perchlorate ($LiClO_4$) were purchased from Sigma-Aldrich (USA); $LiClO_4$ was stored at 80 °C before its use. PLA 2002D pellets were supplied by Nupik International (Polinyà, Spain). Acetonitrile and hexafluoroisopropanol (HFIP) were purchased from Panreac Quimica S.A.U. (Spain).

2.2. Synthesis of PEDOT and COP

Both PEDOT and COP were prepared by anodic polymerization using an Autolab PGSTAT302 N controlled by the NOVA software. Polymerizations were carried out by chronoamperometry (CA) in a three-electrode cell filled with a 0.1 M $LiClO_4$ acetonitrile solution containing 10 mM EDOT for PEDOT or 7 mM EDOT + 3 mM 3DT for COP. In both cases, a constant potential of +1.40 V was applied and the polymerization charge was adjusted to 30 mC. Polished steel AISI 304 sheets (1 × 1 cm^2) were employed as working and counter electrodes, while the

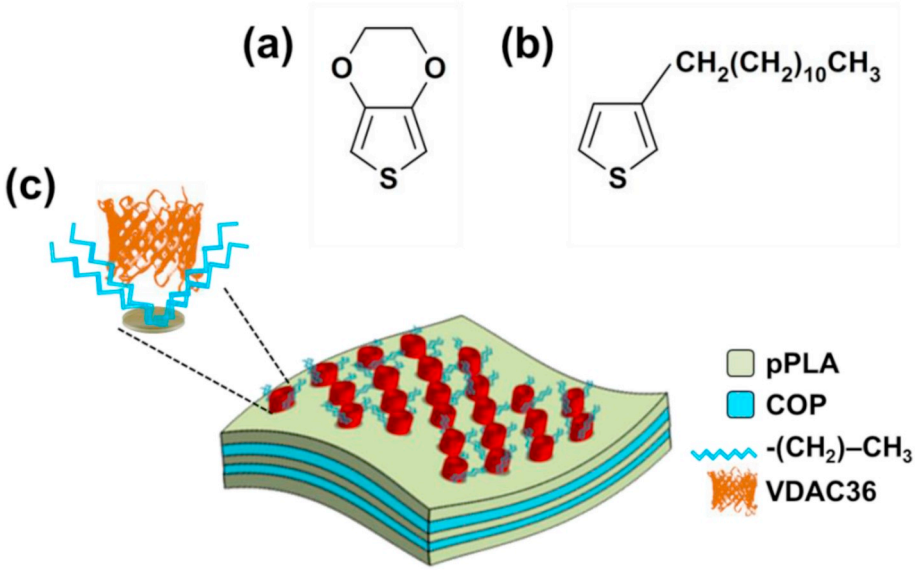

Scheme 1. Chemical structure of (a) 3,4-ethylenedioxythiophene (EDOT) and (b) 3-dodecylthiophene (3DT) repeat units. (c) Structure of 5-pPLA/COP/VDAC. The structure of 5-pPLA/COP corresponds to that obtained before the functionalization of the external pPLA layers with the VDAC36 porin. pPLA refers to the perforated poly (lactic acid) layer, COP is the copolymer of EDOT and 3DT, and VDAC36 is Voltage Dependent Anion Channel protein used in this work.

reference electrode was an Ag|AgCl standard electrode (KCl 3 M).

2.3. Synthesis of 5-layered free-standing films

Films containing 3 layers of pPLA separated by 2 layers of PEDOT or COP were prepared by combining the spin-coating and the anodic polymerization (CA) techniques, following a recently reported procedure [24,25]. In brief, a steel sheet (AISI 304) of 3 × 3 cm^2 was coated with a sacrificial layer of PEDOT:PSS by spin-coating deposition (1200 rpm for 60 s). Then, a PLA:PVA layer was generated onto the sacrificial layer by spin-coating (1200 rpm for 60 s) a 80:20 v/v mixture of PLA (10 mg/mL) and PVA (10 mg/mL) HFIP solutions. The perforated PLA layer (pPLA) was obtained by removing the PVA domains via water etching. The resulting PEDOT:PSS/pPLA bilayer was used as working electrode for the anodic polymerization of COP or PEDOT doped with ClO_4^-, as described before. Afterwards, the following pPLA, COP or PEDOT layers were obtained by iterating this procedure. Then, 5-layered films of composition pPLA/COP/pPLA/COP/pPLA (5-pPLA/COP) and pPLA/-PEDOT/pPLA/PEDOT/pPLA (5-pPLA/PEDOT), still supported onto the PEDOT:PSS-coated steel substrate, were achieved. These supported membranes were easily detached from the metallic substrate by selective elimination of the PEDOT:PSS sacrificial layer. This was achieved by submerging the supported membranes into milli-Q water for 24 h. Finally, 5-layered membranes were completely detached from the steel substrate with the help of tweezers, and converted into self-supported multi-layered films.

2.4. Expression and purification of the VDAC36 protein

Escherichia coli BL21 (DE3) bacteria were transformed to produce 6 His-tagged VDAC36 proteins in inclusion bodies. Bacteria were then lysed and centrifuged to obtain the final pellet corresponding to the non-native proteins. VDAC36, solubilized in 20 mM phosphate pH 8, 1% (w/v) sodium dodecyl sulfate (SDS), was then purified by Ni^{2+} affinity column. VDAC36 was eluted and the buffer was exchanged to the refolded buffer (20 mM phosphate, 60 mM SDS and 1.5 M 2-methyl-2,4-pentanediol (MPD)) with a PD10 desalting column.

2.5. Functionalization of 5-pPLA/COP and 5-pPLA/PEDOT membranes

In order to integrate the porin, the VDAC36 protein was incubated with the free-standing 5-pPLA/COP and 5-pPLA/PEDOT membranes. Films were placed in 1 mL of a protein solution, which contained 0.85 mg/mL VDAC36, 60 mM SDS and 1.5 M MPD, for 12 h at room temperature. The resulting 5-pPLA/COP/VDAC and 5-pPLA/PEDOT/VDAC functionalized membranes were rinsed three times with milli-Q water to remove residues. Blank (non-functionalized) 5-pPLA/COP and 5-pPLA/PEDOT membranes were obtained using the same solution (*i.e.* 60 mM SDS and 1.5 M MPD) but without VDAC36.

The concentration of immobilized protein was determined using a UV–Vis Cary 100 Bio spectrophotometer (Agilent, USA) and a 1 cm length quartz cuvette. The absorbance from 250 to 300 nm was recorded for the protein solutions before and after incubation with the polymeric membranes. The spectra for the solutions after incubation were corrected by subtracting the spectra of the rinsing solutions.

2.6. Characterization

FTIR spectra were recorded on a Nicolet 6700 spectrophotometer by transmittance. For this purpose, the films were removed from the substrate, mixed with KBr and compressed to create discs, which were measured at a 4 cm^{-1} resolution (64 scans).

X-ray photoelectron spectroscopy (XPS) analyses were performed in a SPECS system equipped with a high-intensity twin-anode X-ray source XR50 of Mg/Al (1253 eV/1487 eV) operating at 150 W, placed perpendicular to the analyzer axis, and using a Phoibos 150 MCD-9 XP detector. The X-ray spot size was 650 mm. The pass energy was set to 25 and 0.1 eV for the survey and the narrow scans, respectively. Charge compensation was achieved with a combination of electron and argon ion flood guns. The energy and emission currents of the electrons were 4 eV and 0.35 mA, respectively. For the argon gun, the energy and the emission currents were 0 eV and 0.1 mA, respectively. The spectra were recorded with a pass energy of 25 eV in 0.1 eV steps at a pressure below $6{\cdot}10^{-9}$ mbar. These standard conditions of charge compensation resulted in a negative but perfectly uniform static charge. The C1s peak was used as an internal reference with a binding energy of 284.8 eV. High-resolution XPS spectra were acquired by Gaussian/Lorentzian curve fitting after S-shape background subtraction. The surface composition was determined using the manufacturer's sensitivity factors.

The morphology of the different samples was studied by scanning electron microscopy (SEM). Micrographs were acquired in a Focused Ion Beam Zeiss Neon 40 equipped with an EDX spectroscopy system, operating at 2 or 5 kV, depending on the sensitivity to beam degradation of the studied systems.

The wettability of the NMs was analysed by a sessile water drop method with the equipment OCA 20 (DataPhysics Instruments GmbH, Filderstadt). Images of 5 μL milli-Q water drops onto the samples surfaces were recorded after stabilization (5 s) with the software SCA20. The contact angle (θ) value for each sample was expressed as the average of at least 10 independent measures ± the corresponding standard deviation.

Film thickness and roughness measurements were carried out using a Dektak 150 stylus profilometer (Veeco, Plainview, NY). Conducted using the following settings: tip radius = 2.5 μm; stylus force = 3 mg; scan length = 1000 μm; speed = 33 μm s^{-1}.

2.7. Electrochemical measurements

The electroactivity and electrostability of the new platforms were studied by cyclic voltammetry (CV) through direct measure of the anodic and cathodic areas in the control voltammograms using an Autolab PGSTAT302 N potentiostat controlled by the NOVA software. A three-electrode cell composed by the free-standing NMs as working electrode (WE), platinum wire as counter-electrode, and a reference electrode of Ag|AgCl (KCl, 3 M), was used. More specifically, the free-standing film was hold by an alligator pinch electrode clip and immersed in the electrolyte solution. The surface of film immersed in the solution was 1 cm^2, while the pinch was not in contact with the solution. The electrolyte solution was composed of 0.1 M phosphate buffer saline (PBS) solution (pH 7.4). The initial and final potential was −0.20 V, while the reversal potential was 1.00 V. A scan rate of 50 mV/s was used in all cases. All experiments were repeated three times.

Electrochemical impedance spectroscopy (EIS) measurements were performed using a conventional three-electrode cell and an AUTOLAB-302 N potentiostat/galvanostat operating between the frequency range of 10^5 Hz and 10^{-2} Hz and 10 mV of amplitude for the sinusoidal voltage. All experiments were performed at room temperature with 5-layered free-standing membranes. For the EIS assays the electrolyte solutions were: 0.5 M NaCl, 0.05 M ATP and 0.1 M ATP. Platinum wire was used as counter-electrode, whereas Ag|AgCl saturated (KCl 3 M) was employed as reference electrode.

3. Results and discussion

3.1. Design of 5-layered films

Although both free standing 3- and 5-layered membranes were successfully prepared by alternating pPLA and PEDOT layers and using PEDOT:PSS as sacrificial layer, the choice of the 5-layered system for the current investigation was motivated by its mechanical integrity, which was significantly higher than that of the 3-layered one. More specifically, electrochemical characterization of self-standing 3-layered films

was not possible due to the structural damages induced by the alligator pinch electrode clip. Instead, self-standing 5-layered films were successfully examined by CV and EIS, as is discussed in sections 3.2 and 3.4.

On the other hand, PLA was chosen because of the suitability of this material to prepare perforated layers [26]. Indeed, perforated layer are obtained by selecting two polymers, which are used to induce phase-segregation processes, and by removing the less abundant one by solvent etching. In order to be successful, the two selected polymers should satisfy the following conditions: (i) the two polymers must be immiscible to induce phase segregation processes; (ii) the molecular weight should be similar to promote the formation of nano/micro-features (*i.e.* avoiding that the less abundant polymer acts in another way, for example as plasticizer); (iii) the polymer used to remain in the layer must be insoluble in water, which is the solvent used in this work to remove the less abundant polymer and the sacrificial layer, and to immobilize the VDAC protein at the perforations of the external layers (*e.g.* the utilization of PVA as the most abundant polymer is precluded because of its solubility in water); and (iv) the two polymers used to fabricate the perforated layer must be soluble in a common solvent to facilitate the spin-coating process. Previous studies showed that PLA satisfies all the conditions while other polymers, like for example poly (ethylene glycol) (PEG), fails in some of them (*e.g.* PEG does not favour phase segregation processes because it does not produce enough instabilities at the polymer–polymer interfaces) [26].

3.2. Characterization of the free-standing membranes

Supported 5-pPLA/COP and 5-pPLA/PEDOT free-standing membranes were prepared by alternating spin-coated pPLA and electropolymerized conducting COP or PEDOT layers, as described in the Methods section. When spin-coating the 1st pPLA layer of pPLA onto the PEDOT:PSS sacrificial layer (thickness: 302 ± 3 nm), the strategy of using two immiscible polymers (PLA:PVA, 80:20 v/v) resulted in the formation of segregated pseudo-spherical domains, as shown in Fig. 1a. The diameter of such features was adjusted to the entire film thickness by regulating the operational conditions of the spin-coating process (*i.e.* time and angular speed) and the concentration of the less abundant polymer (PVA) in the feeding mixture. Afterwards, PVA domains were successfully removed by solubilizing them in water, as explained in the experimental procedure, and perforations of 462 ± 219 nm in diameter were achieve (Fig. 1b). It is worth noting that the formation of such perforations is required for successful electropolymerization of the 2nd conducting layer (*i.e.* the access of the 3DT and EDOT monomers to the conducting PEDOT:PSS sacrificial layer, which acts as working electrode in the electropolymerization, is possible because of the perforations.

The surface morphology of COP and PEDOT in the 2nd layers, which was checked by SEM (Fig. 1c and d, respectively), is very similar to that displayed by the CPs directly generated onto steel substrates (Figs. S1b and S1c). This demonstrates that perforations were successfully formed by phase segregation in the 1st pPLA layer. The absence of perforations in the PLA layer was found to preclude the formation of homogeneous CP layers since the microstructure of the former hinders the action of the PEDOT:PSS working electrode in the anodic polymerization process [25].

SEM micrographs displayed in Fig. 1e and f shows the morphology of the 3rd pPLA layer deposited onto the 2nd COP and PEDOT layers, respectively. In both cases rounded-shape perforations with average diameter 245 ± 96 nm and 232 ± 127 nm, respectively, are observed. As is shown in Fig. 1g and h, the 4th COP and PEDOT layers were successfully generated onto the 3rd PLA layer, evidencing that 3DT and/or EDOT monomers were able to access the CP chains deposited in the 2nd layer through the perforations of the 3rd pPLA layer.

Fig. 1i and j shows the morphology of the outer pPLA layer (*i.e.* the fifth layer of the 5-pPLA/COP and 5-pPLA/PEDOT bioactive membranes). In this case the average diameter of the perforations increased to 321 ± 150 nm and 403 ± 294 nm, respectively. The diameter of the perforations in the 3rd and 5th pPLA layers is affected by the morphology and topography of the previous CP layers. Indeed, the diameter of the perforations is smaller in 5-pPLA/COP than in 5-pPLA/PEDOT since the surface roughness is lower for COP layers than for PEDOT layers (Figs. S2a–b). Besides, the 4th COP or PEDOT layer can be observed through the perforations of the outer pPLA layer in Fig. 1i and j.

The total thickness of 5-pPLA/COP films is 998 nm ± 57 nm, while that of 5-pPLA/PEDOT is 741 nm ± 23 nm. These values are consistent with the sum of the thicknesses obtained for single-layered films: COP and PEDOT supported onto steel (*i.e.* 381 ± 59 and 171 ± 26 nm, respectively) and pPLA spin-coated using a 80:20 v/v PLA:PVA mixture (*i.e.* 170 ± 14 nm) [26]. Similarly, the surface roughness is significantly higher for 5-pPLA/COP (Rq = 418 nm ± 76 nm) than for 5-pPLA/PEDOT (Rq = 185 nm ± 50 nm), which differs from the results discussed in the Supplementary Information for the CPs directly generated onto steel. This has been attributed to the templating effect induced by the alkyl chains of the COP when it grows onto elastic pPLA membranes. On the other hand, the water wettability, which is mainly controlled by the outer pPLA layer, is pretty similar for the two 5-layered systems ($\theta = 88° \pm 6°$ and $85° \pm 8°$ for 5-pPLA/PEDOT and 5-pPLA/COP, respectively).

The electroactivity and electrostability of the two 5-layered membranes have been examined to confirm the efficiency of the oxidation-reduction processes when insulating PLA sheets separate the CP layers. Fig. 2a compares the cyclic voltammograms recorded in PBS 0.1 M for free-standing 5-layered membranes. As expected, the electrochemical activity is lower for free-standing membranes than for CP films supported on steel substrate (Fig. 2b) due to the presence of pPLA layers. The loss of electrochemical activity (LEA) after 25 consecutive redox cycles is lower for 5-pPLA/PEDOT than for 5-pPLA/COP (LEA = 1% and 17%, respectively).

Additionally, the robustness and flexibility of the free-standing membranes were observed by the manipulation of the films. Then, Fig. 2c shows digital camera images of a 5-pPLA/COP membrane, which was fabricated and detached using the procedure described in the Methods section. The sequence of images (Fig. 2c1-2c4) reveals that the free-standing films are not only manageable and robust but they are also very flexible. Fig. 2c– shows the aspiration process of a film, with an area of 0.5 cm^2, floating in water into a pipette with a tip diameter of 1.5 mm. Due to its outstanding flexibility, the 5-layered membrane does not obstruct the pipette tip but, instead, is completely introduced and delivered from it without damage (Figs. 2c–3). After release into the solvent, the film slowly tends to recover its original shape (Figs. 2c–4). Then, the film can be dried for manipulation without damaging its structure.

The aspiration-release-shape recovery-drying process can be repeated at least five times without any damage to the membrane. The same behaviour was obtained for 5-pPLA/PEDOT films (not shown). The mechanical stability of the 5-pPLA/COP and 5-pPLA/PEDOT membrane is demonstrated in Fig. 2d, which shows representative low magnification SEM micrographs recorded after two consecutive aspiration-release-shape recovery-drying cycles. As is shown, no structural fail was detected at the surface of the films in these or any of the recorded micrographs. This mechanical stability is consistent with elastic modulus of 5-pPLA/PEDOT, 3.4 GPa, which was determined by nanoindentation [24]. The latter value is very similar to that typically found for PLA tensile using strain-stress assays, reflecting that the mechanical stability of 5-layered membranes are provided by the three pPLA nanolayers.

3.3. Bioactivation of the free-standing membranes with porin

In order to prove the successful immobilization of the VDAC36 protein on the membranes, the chemical structure of the bioactive platforms was investigated by XPS. Table 1 compares the surface atomic compositions of 5-pPLA/COP/VDAC and 5-pPLA/PEDOT/VDAC with

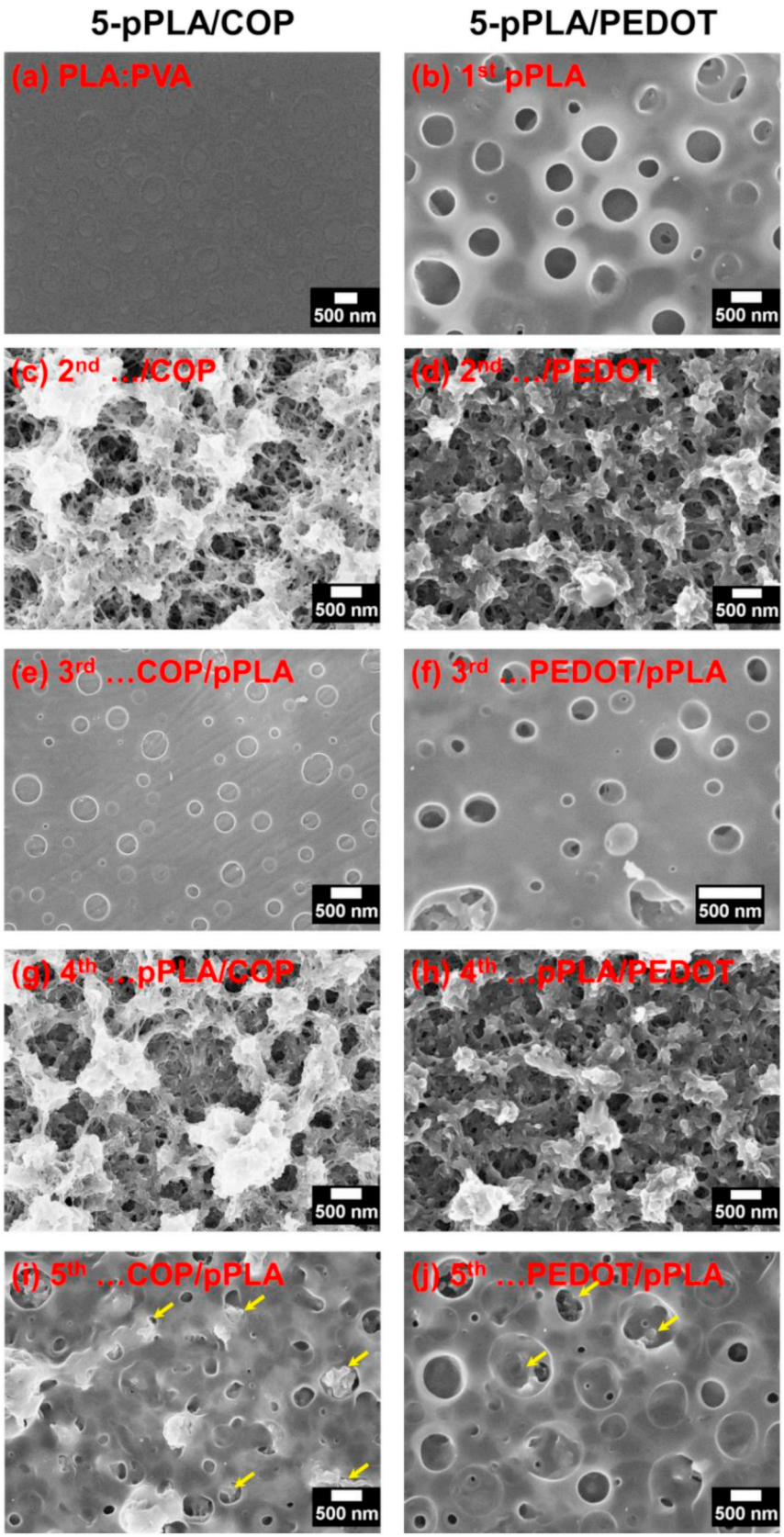

Fig. 1. SEM images of the five layers involved in 5-pPLA/COP and 5-pPLA/PEDOT systems. (a) spin-coated 80:20 PLA:PVA layer. (b) 1st pPLA layer after elimination of PVA by water etching. 2nd (c) COP and (d) PEDOT layer electropolymerized onto the 1st pPLA layer. 3rd pPLA layer spin-coated onto the 2nd (e) COP and (f) PEDOT layer. 4th (g) COP and (h) PEDOT layer electropolymerized onto the 3rd pPLA layer. 5th pPLA layer spin-coated onto the 4th (i) COP and (j) PEDOT layer. Arrows in (i) and (j) indicate the CP layer observed under the outer pPLA layer. pPLA refers to the perforated poly (lactic acid) layer, PEDOT is poly (3,4-ethylenedioxythiophene) and COP is the copolymer of 3,4-ethylenedioxythiophene and dodecylthiophene.

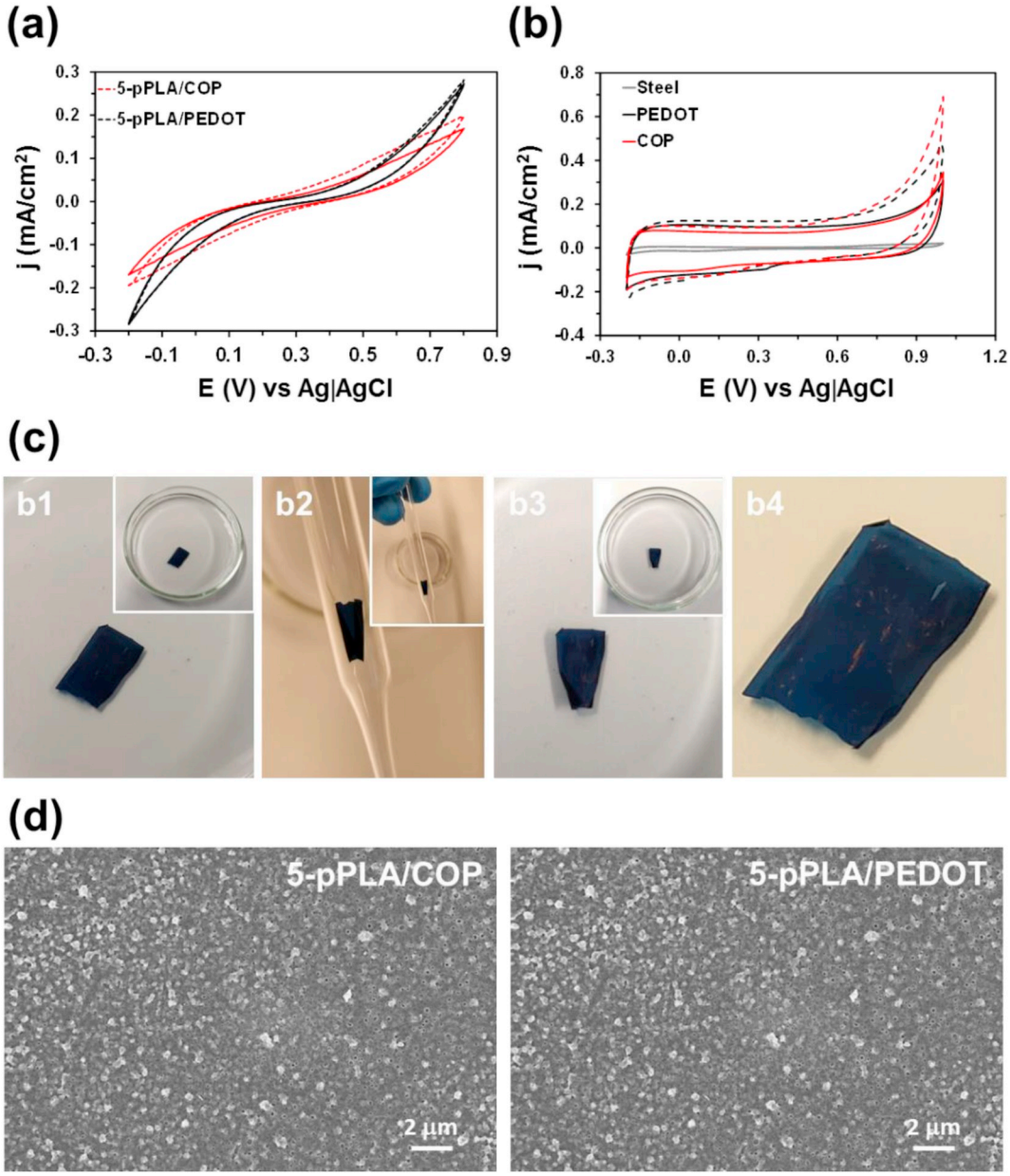

Fig. 2. First control voltammogram (dashed lines) and voltammogram curve after 25 consecutive oxidation–reduction cycles (solid lines) in PBS 0.1 M for free-standing 5-pPLA/COP and 5-pPLA/PEDOT films. (b) First control voltammogram (dashed lines) and voltammogram after 25 consecutive oxidation–reduction cycles (solid lines) in 0.1 M PBS for steel, COP and PEDOT. (c) Digital camera images of a 5-pPLA/COP free-standing film immersed in water (c1); aspired film floating in water into a pipette (c2); aspect of the film while it recovers the shape once it has been released into the water solution (c3); and dried film after having completely recovered the shape (c4). (d) Representative SEM micrographs of 5-pPLA/COP and 5-pPLA/PEDOT free-standing membranes showing that, after two aspiration-release-shape recovery-drying cycles, no structural damage is detected at the surface. pPLA refers to the perforated poly (lactic acid) layer, PEDOT is poly (3,4-ethylenedioxythiophene) and COP is the copolymer of 3,4-ethylenedioxythiophene and dodecylthiophene.

the corresponding controls, which were prepared incubating the free-standing membranes in a 60 mM SDS and 1.5 M MPD solution without protein. Whilst the penetration of X-ray radiation using the conditions described in Methods section is expected to be ~10 nm, here the penetration is unknown due to both the nanometric thickness of the layers and the filling of the perforations of the outer pPLA layers (see below). The N 1s detected in the composition of 5-pPLA/COP and 5-pPLA/PEDOT controls has been attributed to the usual N_2 contamination from air. However, the N 1s increases from 0.63 to 0.64% in the control samples to 0.89% and 0.85% in 5-pPLA/COP/VDAC and 5-pPLA/PEDOT/VDAC, respectively, supporting the successful integration of the VDAC36 onto the surface of the films.

Fig. 3 displays the high-resolution XPS spectra in the S 2p region for functionalized and control films, which show the spin-split sulphur coupling S $2p_{3/2}$ and S $2p_{1/2}$ with a separation of 1.2 eV. The spectrum recorded for the 5-pPLA/COP control sample reveals two peaks, which transform into six (A–F) after deconvolution (3 for S $2p_{3/2}$ and 3 for S $2p_{1/2}$). The peak at 167.9 eV (after deconvolution A and B at 167.7 and 168.9 eV, respectively) corresponds to the $-SO_3^-$ of the SDS used in the incubation buffer. The second peak at 163.7 eV has been associated to the signals of the thiophene rings: the C–S–C bond (C and D at 163.2 and 164.4 eV, respectively) and its homologous with positively charged sulphur, $C–S^+–C$ (E and F at 164.2 and 165.4 eV, respectively) [27]. The same trends are observed in the spectrum obtained for the

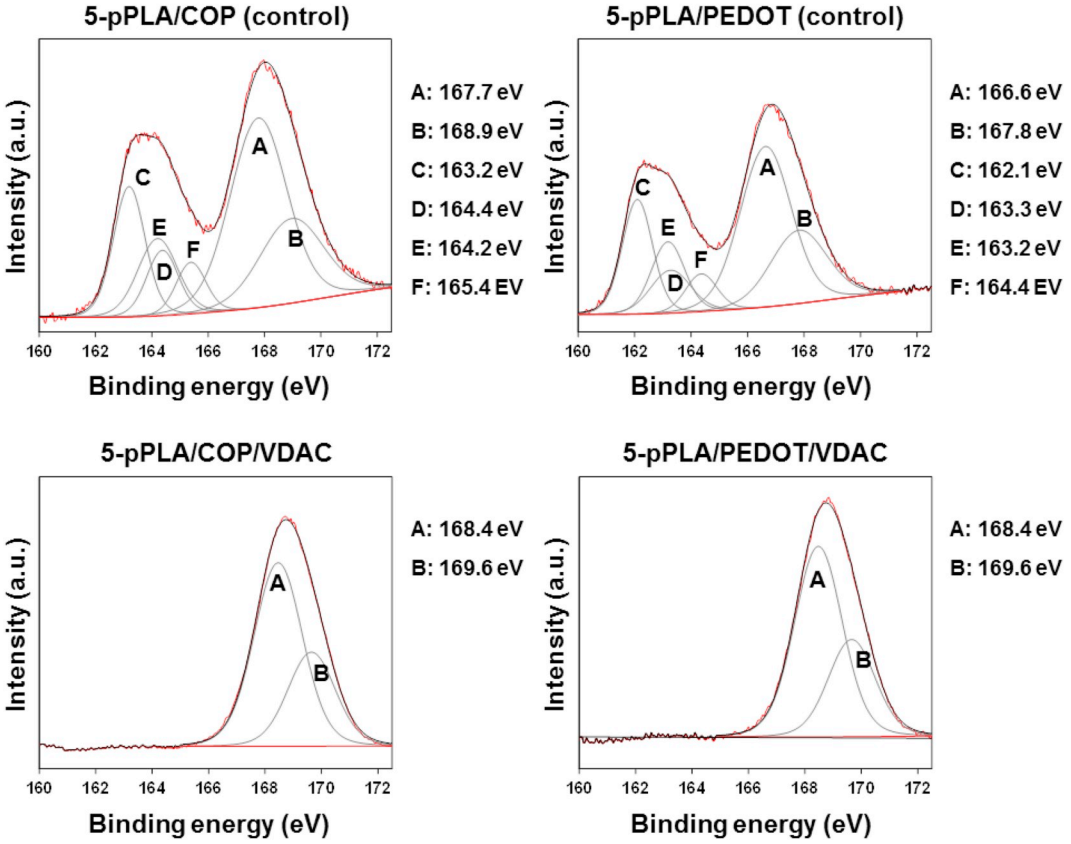

Fig. 3. High-resolution XPS spectra in the S 2p region for 5-pPLA/COP and 5-pPLA/PEDOT control films (*i.e.* samples incubated in a 60 mM SDS and 1.5 M MPD aqueous solution without protein) and functionalized 5-pPLA/COP/VDAC and 5-pPLA/PEDOT/VDAC films (*i.e.* samples incubated in a 60 mM SDS and 1.5 M MPD aqueous solution with 0.85 mg/mL of protein). The recorded spectrum is displayed in black, the curves coming from the deconvolution are shown in grey, and red lines correspond to the background and profile obtained by summing the curves from deconvolution. pPLA refers to the perforated poly (lactic acid) layer, PEDOT is poly (3,4-ethylenedioxythiophene), COP is the copolymer of 3,4-ethylenedioxythiophene and dodecylthiophene, and VDAC is the Voltage Dependent Anion Channel protein. (For interpretation of the references to colour in this figure legend, the reader is referred to the Web version of this article.)

5-pPLA/PEDOT control, the only difference with respect to 5-pPLA/COP being that the binding energy of the peaks from the experimental profile and from deconvolution decrease by ~1.1 eV. For both control films, the sulphur content at the surface originating from SDS was slightly higher than from the CP (Table S2).

Interestingly, biofunctionalized 5-pPLA/COP/VDAC and 5-pPLA/PEDOT/VDAC films do not show the peak associated to the CP. Thus, the only detected peak, which appears at 168.8 eV, corresponds to the detergent of the solution used for the incubation of the protein. As shown in the SEM micrographs discussed above (Fig. 1), the CP layers are accessible through the perforations in the outer pPLA layers before functionalization. Accordingly, the disappearance of the thiophene peak from the XPS spectra in the S 2p region indicates that the protein fills the perforations and adsorbs on the underlying CP layer, occulting the presence of COP or PEDOT. Although these results demonstrate the immobilization of VDAC36 inside the perforations, looking for the accessible CP chains, its adsorption onto the PLA at surface of the outer layers cannot be ruled out. However, it is well-known that the physical immobilization of proteins and protein aggregates on flat surfaces, as for example the spin-coated PLA, is more difficult than onto rough surfaces, as for example the electropolymerized CP [28]. The immobilization of the VDAC36 protein was further investigated by FTIR spectroscopy, results being described in the Supplementary Information (Fig. S3).

In order to quantify the amount of VDAC36 retained by the films, the solutions containing the protein were analysed by UV absorbance. More specifically, the absorbance at 280 nm was determined for the protein solution before and after films incubation, correction of the rinsing solutions being applied to the latter. The VDAC36 M extinction coefficient, calculated by the ProtParam software, is 20,400 $M^{-1}cm^{-1}$ [29]. The original concentration was 0.847 mg/mL. After incubation, the concentrations were 0.825 and 0.830 mg/mL for the 5-pPLA/COP and 5-pPLA/PEDOT, respectively. Accordingly, the quantity of protein retained by the 5-pPLA/COP/VDAC and 5-pPLA/PEDOT/VDAC films is 2.704 and 2.043 $\mu g/cm^2$, respectively. This result indicates that the retention of protein increased by 32% when 3DT units were incorporated to the CP layers, demonstrating the importance of the lipid-like environment for the incorporation of the porins to artificial membranes.

This biomimetic effect has been attributed to the very different hydrophobic degrees co-existing in COP chains. Thus, the water contact angles measured for PEDOT [30] and unsubstituted polythiophene [31] films, both prepared by anodic polymerization, are 82°±2° and 89°±2°, respectively, these values being at the interface of hydrophilic and hydrophobic behaviors. In contrast, the water contact angle for dodecyl chains grafted to silane is near to 165 °C [32], close to the superhydrophobicity. Thus, hydrophobicity was found increase very rapidly when the grafted alkyl groups involve at least 12 carbon atoms, which is fulfilled in COP, and the density of dodecyl groups (*i.e.* amount by surface unit) is high enough [32]. Obviously, in the case of COP the density of 3DT units is not sufficient to produce superhydrophobicity but it is enough to facilitate the formation of two distinct environments, mimicking lipids and increasing the retention of protein by 32%.

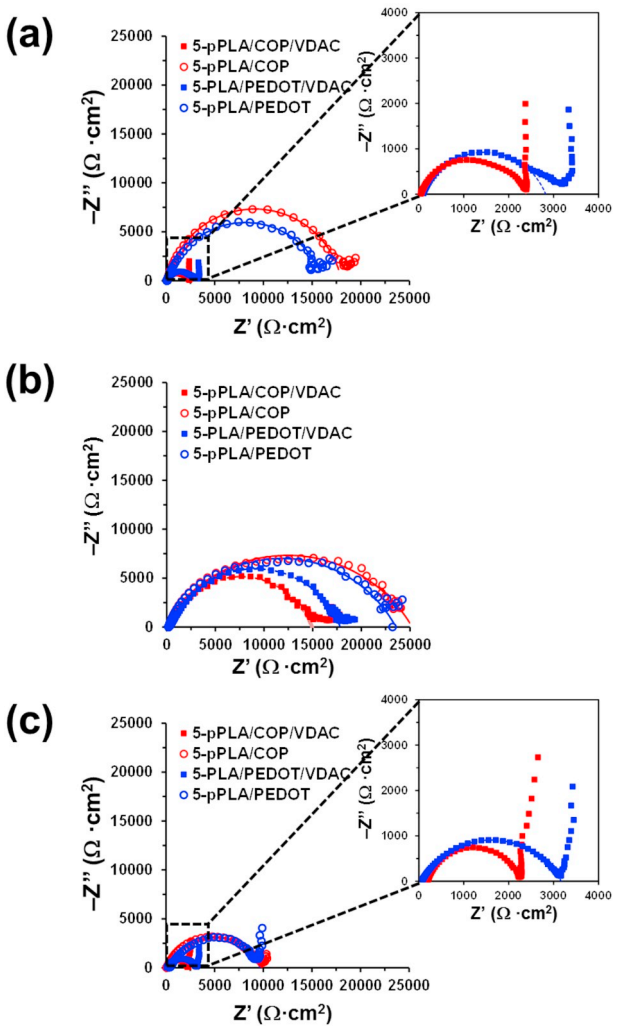

Fig. 4. Nyquist plots for non-functionalized (control) and VDAC36-functionalized free-standing 5-layered membranes in (a) NaCl 0.5 M, (b) ATP 0.05 M and (c) ATP 0.1 M aqueous solutions. VDAC36 is Voltage Dependent Anion Channel protein used in this work.

Table 1
Atomic percent composition (C 1s, O 1s, S 2p and N 1s) obtained by X-ray photoelectron spectroscopy (XPS) for control and functionalized free-standing films.

Sample	C 1s (%)	O 1s (%)	S 2p (%)	N 1s (%)
5-pPLA/COP (control)	57.71	35.24	6.42	0.63
5-pPLA/COP/VDAC	69.66	22.30	7.48	0.89
5-pPLA/PEDOT (control)	66.05	27.27	6.05	0.64
5-pPLA/PEDOT/VDAC	63.30	30.03	5.62	0.85

3.4. Effectiveness of ion transport across 5-pPLA/COP/VDAC by electrochemical impedance spectroscopy measurements

EIS measurements were performed to study the effectiveness of the protein activity on the ion transport across the bioactivated free-standing membranes. Both functionalized and control free-standing membranes were considered in this step by using three different electrolyte solutions: NaCl 0.5 M, ATP 0.05 M and ATP 0.1 M. The NaCl 0.5 M solution was selected as the standard to assess the membrane resistance and for further comparison to the results from previous works involving biomimetic membranes made of polymers and porins. Instead, the ATP electrolyte was examined to take profit of the main VDAC function *in vivo*, which is the transport of this metabolite across the mitochondrial membranes. Accordingly, 5-pPLA/COP/VDAC and, especially, 5-pPLA/PEDOT/VDAC films are expected to behave as biosensors of relevant cellular compounds. The results were expressed as solution resistance (R_s), membrane resistance (R_M) and membrane capacitance, *i.e.* the capacitance of real systems (CPE, constant phase element), by using the simple Randles electrical circuit.

Fig. 4 displays the collected impedance (Z) data as a Nyquist plot for the three studied electrolyte solutions, while the corresponding Bode plots (both magnitude and phase angle results) are provided in Figs. S4–S6. Nyquist plots for bioactivated membranes obtained using 0.5 M NaCl and 0.1 M ATP solutions show a low capacitive semicircle in the high-frequency range and a straight ascending vertical line (almost 90° to the real axis and overlapping the semicircle) in the low-frequency range. This vertical line combines the effects of mass capacitance, which is ascribed to PEDOT layers, and the diffusion of electrolytes [33]. On the other hand, Nyquist plots for control 5-pPLA/COP and 5-pPLA/PEDOT membranes consist of a large semicircle (*i.e.* high capacitance), which extends from the high frequency to the low frequency range. A similar behaviour is observed for functionalized membranes when a 0.05 M ATP solution is employed, reflecting a concentration-dependent behaviour.

The diameter of the semicircle, which is very sensitive to the microstructure of the membrane, is directly proportional to the membrane resistance. Accordingly, the results displayed in Fig. 4 indicate that the incorporation of the VDAC36 protein inside the pores considerably increases the membrane conductivity. Besides, the Nyquist plots obtained for non-functionalized membranes in 0.5 M NaCl and 0.05 M ATP do not show any straight line ascending in the low frequency range, indicating that diffusion is hindered in these systems.

The impedance of the Bode plot shows that, in all cases, the solution resistance dominates at high frequency, while the sum of the solution resistance and the membrane resistance predominates at low frequency. Accordingly, in the low frequency range, functionalized and control membranes show differences in the electrolyte–membrane interface. In the log |Z| *vs* log f plots (Figs. S4–S6), a shoulder appears between 10^2 and 10^4 Hz for functionalized membranes, which corresponds to the parallel association of the membrane resistance and the membrane capacitance. Such a shoulder is associated to one time constant in the phase angle Bode plot, and it appears at lower log f values for control membranes than for bioactivated membranes, reflecting the role of the porin in the diffusion of ions.

The noisy points that appear in the low frequency range of Nyquist plots, especially for the ATP 0.05 M solution in the low-frequency range, which has been associated to the free-standing nature of the membrane. This makes difficult the fitting of the experimental data to a proposed electric equivalent circuit (EEC) for explaining the whole EIS profiles. In order to overcome this drawback, the simplified Randles EEC (Fig. 5a) has been used to obtain the electrolyte resistance (R_s), the membrane resistance (R_M), which represents the ability of the membrane to impede ion transport at the interface, and the double layer capacitance (C_{dl}) in parallel with R_M, which can store only charge and ion movement. The role played by the C_{dl} in ion-exchange membrane systems constituted by the membrane and two diffusion boundary layers adjacent to the membrane was recently analysed by Moya [34]. At high frequencies, C_{dl} has very low impedance values and the main contribution comes from R_s (*i.e.* the solution acts as an Ohmic resistor). Accordingly, the semicircles start at R_s (Fig. 4). At low frequencies, C_{dl} has very high impedance values and all the current goes through R_M. Therefore, the impedance contribution at the point where the right end of the semi-circle intercepts the y-axis is $R_s + R_M$. C_{dl} has been modelled as a constant phase element (CPE_{dl}), which represents the capacitance of real systems, as explained above. Thus, CPE_{dl} represents the ability of the system, taking into account the contribution of all membrane components. In addition to the heterogeneity of the surface (*i.e.* roughness, porosity, reactivity), the CPE impedance (Z_{CPE}) is related to non-uniform diffusion across the

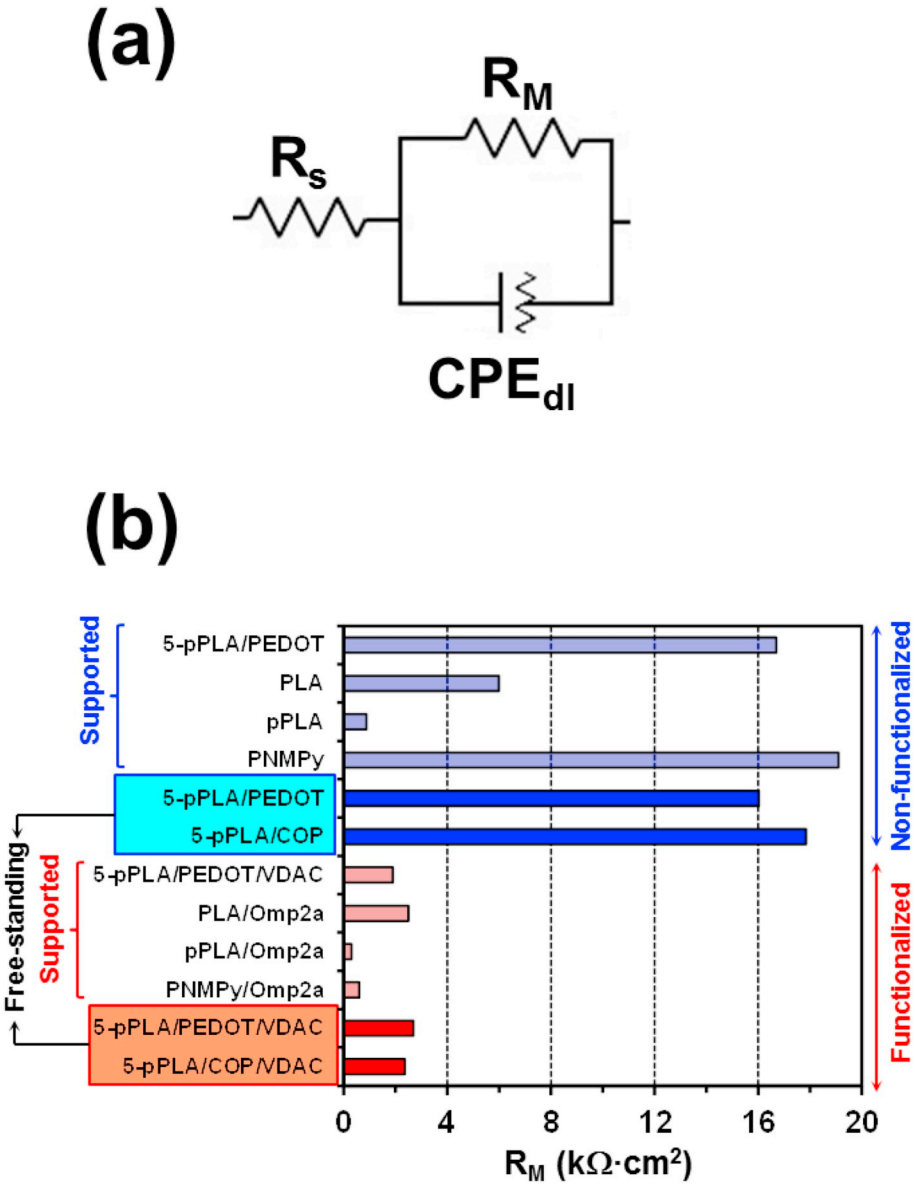

Fig. 5. Randles EEC used to fit the experimental data in the semicircle of the Nyquist plots. (b) Comparison of the R_M values obtained in this work for free-standing 5-pPLA/COP/VDAC and 5-pPLA/PEDOT/VDAC, 5-pPLA/COP and 5-pPLA/PEDOT membranes with those obtained for supported functionalized and non-functionalized organic membranes. R_M values were determined by EIS using a NaCl 0.5 M electrolyte solution in all cases with exception of the supported PNMPy and PNMPy/Omp2a membranes, for which a NaCl 0.14 M electrolyte solution was used. PLA and pPLA refers to the non-perforated and perforated poly (lactic acid) layers, respectively, PEDOT is poly (3,4-ethylenedioxythiophene), COP is the copolymer of 3,4-ethylenedioxythiophene and dodecylthiophene, PNMPy is poly (N-methylpyrrole), Omp2a is an outer membrane protein, and VDAC refers to the Voltage Dependent Anion Channel protein used in this work.

interface. Mathematically, Z_{CPE} is expressed as $[Q\cdot(i\cdot\omega)^n]^{-1}$, where Q is the CPE parameter, i the imaginary unit, ω the angular frequency, and n the CPE exponent representing a pure capacitor ($n = 1$), a pure resistor ($n = 0$) or a diffusion process ($n = 0.5$) [35]. Both R_M and CPE_{dl} are expected to include the contribution of the VDAC36-integrated protein for 5-pPLA/COP/VDAC and 5-pPLA/PEDOT/VDAC membranes.

The parameters obtained from the fitting of the experimental data in the semicircle to the Randles EEC are listed in Table 2. The presence of COP in membranes slightly increases the resistance of non-functionalized membranes, as R_M is higher for 5-pPLA/COP than for 5-pPLA/PEDOT by 11%, 7% and 4% in NaCl 0.5 M, ATP 0.05 M and ATP 0.1 M, respectively. This has been attributed to differences in the electrical conductivity of the CP matrices (*i.e.* the electrical conductivity is lower for COP than for PEDOT). The low conductivity of poly (3-alkylthiophene)s in comparison to PEDOT was previously studied, being attributed to the self-rigidification of the thiophene ring in the latter [36]. More specifically, in PEDOT the π-conjugation induced by the geometric restrictions imposed by the cyclic substituent and the electron-donating effects of the oxygen atoms produce a gain in aromaticity and favour electrostatic interactions when planarity is reached. This gain is not achieved in poly (3-alkylthiophene)s, which reduces the aromaticity and the effective conduction pathways. On the other hand, the capacitive behaviour of the non-functionalized films is very similar, independently of the CP used for the 2nd and 4th layer.

After the incorporation of the VDAC porin, the diameter of the semicircle decreases drastically. This reflects an enhanced flow of charges at the electrolyte–membrane interface, as well as an increment of current crossing the nanomaterial, both phenomena leading to a great reduction of R_M when compared to the non-functionalized systems. The membrane resistance decay increases with the conductivity of the electrolyte solution. Moreover, the initial hypothesis that the incorporation of 3DT units would help to retain a higher amount of protein and to keep it in its active form is fully supported by the EIS results. Indeed, the combination of VDAC36 with COP leads to a greater resistance reduction than when combined with PEDOT. Despite these benefits, it should be noted that the reduction in resistance could be even greater by controlling the orientation of the protein immobilized in the pores. However, this is a challenge that is not easy to tackle.

Fig. 5b compares the resistance of free-standing membranes studied in this work with that of supported membranes reported in literature,

Table 2
Resistance of the electrolytic solution (R_s), resistance of the membrane (R_M) and constant phase element (CPE) with the exponent parameter *n* for the different functionalized and non-functionalized (control) free-standing 5-layered membranes.[a)] pPLA refers to the perforated poly (lactic acid) layer, PEDOT is poly (3,4-ethylenedioxythiophene), COP is the copolymer of 3,4-ethylenedioxythiophene and dodecylthiophene, and VDAC refers to the Voltage Dependent Anion Channel protein used in this work.

Sample	R_s ($\Omega \cdot cm^2$)	R_M ($k\Omega \cdot cm^2$) [b)]	CPE ($\mu F \cdot cm^{-2} \cdot s^{n-1}$)	*n*
NaCl (0.5 M)				
5-pPLA/COP/VDAC	102	2.36 (87%)	1.07	0.732
5-pPLA/COP	102	17.85	4.61	0.876
5-pPLA/PEDOT/VDAC	102	2.69 (83%)	0.53	0.768
5-pPLA/PEDOT	102	16.03	4.50	0.814
ATP (0.05 M)				
5-pPLA/COP/VDAC	431	14.40 (43%)	0.12	0.790
5-pPLA/COP	431	25.12	5.00	0.689
5-pPLA/PEDOT/VDAC	431	17.40 (26%)	0.16	0.766
5-pPLA/PEDOT	431	23.52	4.64	0.679
ATP (0.1 M)				
5-pPLA/COP/VDAC	202	2.07 (78%)	0.53	0.794
5-pPLA/COP	202	9.53	4.72	0.674
5-pPLA/PEDOT/VDAC	202	3.11 (66%)	0.35	0.751
5-pPLA/PEDOT	202	9.18	4.60	0.653

[a)] Data were obtained by fitting the semicircle of the Nyquist plots fom EIS measurements to a simple Randles circuit. [b)] The percentages in parenthesis indicates the resistance reduction for the membranes with the same CP after incorporation of the VDAC36 protein.

before and after functionalization with porins. In all cases, R_M was determined by EIS using NaCl as electrolyte (*i.e.* a NaCl 0.5 M solution was selected for all studies with exception of PNMPy and PNMPy/Omp2a, in which a NaCl 0.14 M solution was used). The resistance of the free-standing 5-layered membranes functionalized with VDAC36 is slightly higher than that previously obtained for supported PNMPy/Omp2a [11] and npPLA/Omp2a [12] membranes (R_M = 0.6 and 0.3 kΩ cm^2, respectively). The latter were built by immobilizing the pore-forming Omp2a protein over a PNMPy film electropolymerized onto a rigid steel electrode and over a npPLA film spin-coated onto a ITO substrate, respectively. The thickness of the PNMPy and npPLA films (~300 and 110 ± 7 nm, respectively) was reported to be similar to those of the CP and pPLA layers in the 5-layered membrane developed in this work. Hence, the higher resistance of the free-standing films has been essentially attributed to the fact that supported membranes do not suffer drawbacks associated to the manipulation of thin free-standing films, like the folds inducing local changes in the resistance. In order to confirm this assumption, the R_M of supported 5-pPLA/PEDOT/VDAC and 5-pPLA/PEDOT membranes were determined by EIS in NaCl 0.5 M solution. As shown in Fig. 5b, the resistances measured for supported 5-pPLA/PEDOT/VDAC (R_M = 1.9 kΩ cm^2) and 5-pPLA/PEDOT (R_M = 16.7 kΩ cm^2) were slightly lower and higher, respectively, than those obtained for the corresponding free-standing film. This indicates that the self-supporting capacity of 5-layered membranes only produces a small change in the resistance.

On the other hand, Table 2 shows that, independently of the electrolyte solutions, CPE_{dl} decreases after the integration of VDAC36, indicating that protein-promoted ion diffusion causes a loss of capacitance. For the study in 0.5 M NaCl, the increasing contribution of the diffusion process is also reflected by the reduction of the *n* exponent (see Z_{CPE} expression). The opposite behaviour is observed in the ATP solutions for which the *n* value is higher for the functionalized membranes than for the control ones. This difference has been attributed not only to the ATP diffusion coefficient, which is much lower than that of Cl^- (3.10^{-6} and 2.03 10^{-5} cm^2/s for ATP and Cl^-, respectively) but also to the binding affinity of ATP with VDAC proteins [37–39].

It is worth noting that the working conditions of 5-layered membranes functionalized with VDAC36 are restricted by the stability of the β-barrel structure, which is responsible of the channel activity. In general, the stability of β-barrel channels is pH and temperature dependent. Thus, it has been observed that the stability of VDAC's β-barrel and, therefore, the transport of metabolites across the pore decrease at low pH and is restored at pH 7 [40]. Besides, it has been proved that the structure of OMPs used for biomimetic membranes remains stable up to temperatures higher than 100 °C without losing properties [41].

On the other hand, the economic viability of producing polymeric flexible devices functionalized membrane proteins is limited by the cost of the latter. This drawback can be drastically mitigated utilizing optimized expression bacterial systems for the production of membrane proteins. In last years, membrane proteins have been often overexpressed in *Escherichia coli* bacteria [42,43], which were selected because of the following advantages: (i) easy DNA transformation; (ii) fast growth and high cell density cultures; (iii) inexpensive culture costs and (iv) high yield of overexpression. These biotechnological techniques are expected to contribute the implementation of biomimetic membranes as routine devices in technological and biomedical applications.

3.5. Permselectivity measurements

The influence of the VDAC porin on the ion permselectivity was examined considering the 5-pPLA/COP/VDAC and 5-pPLA/COP membranes fixed to porous support (glass frit discs of 25 mm in diameter having a non-porous peripheral adage of 6 mm, 3.65 in thickness and average pore size of 10–16 μm) in a two-compartment cell with a circular exposed area of 4.5 cm^2. A 0.1 M NaCl solution was used for this study, as is usual in this kind of assays, since the transport number and the diffusion coefficient of ATP are unknown. Complete description of the set-up, the cell and the porous support is provided in previous work [44]. Both compartments were filled with a 0.1 M NaCl solution and, after fix the membrane to the porous support, chronoamperometric measurements were performed using steel AISI 316L sheets as working and counter electrodes while an Ag|AgCl electrode was used as reference electrode.

The transition time for an ideally permselective membrane was calculated using Eqn (1) [45]:

$$P = \frac{|z|FD^{0.5}\pi^{0.5}C}{2(1-t_i)\frac{I}{A}\tau^{0.5}} \quad (1)$$

where *P* is the permselectivity, *z* is the absolute charge of the chloride ion, F is the Faraday constant (96,485 A s/mol), *D* is the diffusion coefficient ($1.48 \cdot 10^5$ cm^2/s), t_i is the transport number (0.604) of the chloride ion in 0.1 M NaCl, *C* is the concentration of chloride ions (0.1 M), *I* is the applied current (10 mA in this case), *A* is the exposed membrane area, and τ is the transition time for the real membrane, which was measured as the inflection point of the chronopentiometric curve.

The permselectivity, normalized with respect to the porous support (i.e. *P* = 100% for the porous support), is 62% ± 6% and 89% ± 7% for 5-pPLA/COP and 5-pPLA/COP/VDAC, respectively. A membrane with permselectivity of 0% shows no ion selectivity compared to the solution phase, while a permselectivity of 100% means the co-ion flux through the membrane is 0. Our results clearly show that the incorporation of the VDAC36 protein has a positive effect in the permeselectivity.

4. Conclusions

In the present study, a free standing and conducting polymeric membrane with porin protein immobilized has been developed and proved to be efficient for transport of ATP and NaCl, for first time. The VDAC36 protein has been immobilized at the external layers of free-standing 5-pPLA/COP membranes. The retention of such protein has

been found to be higher for COP- than for PEDOT-containing membranes, indicating that the dodecyl alkyl chains successfully mimic the lipophilic environment of cell membranes. The incorporation of the porin, which retains its function, has induced important electrochemical changes in the membrane resistance and capacitance, promoting the diffusion of ions, especially of ATP. In conclusion, the hybrid system obtained by combining synthetic polymers (CP and biodegradable PLA) and porin proteins is well-suited for the development of flexible membrane biosensors with fully functional transmembrane ion channels. The new platform is fully free-standing and flexible and can be applied in many biomedical technologies, opening new frontiers for the future development of high-throughput screening assays.

Declaration of competing interest

The authors declare that they have no known competing financial interests or personal relationships that could have appeared to influence the work reported in this paper.

CRediT authorship contribution statement

Brenda G. Molina: Conceptualization, Investigation, Validation, Formal analysis, Writing - original draft, Visualization. **Maximilien Lopes-Rodrigues:** Investigation, Validation, Formal analysis, Writing - original draft, Visualization. **Francesc Estrany:** Methodology, Validation, Supervision. **Catherine Michaux:** Conceptualization, Resources, Funding acquisition. **Eric A. Perpète:** Conceptualization, Resources, Funding acquisition. **Elaine Armelin:** Methodology, Validation, Supervision. **Carlos Alemán:** Conceptualization, Formal analysis, Resources, Writing - review & editing, Funding acquisition.

Acknowledgements

Authors acknowledge MINECO-FEDER (RTI2018-098951-B-I00) and Agència de Gestió d'Ajuts Universitaris i de Recerca (2017SGR359 and FI grant to ML-R) for financial support. Support for the research of C.A. was received through the prize "ICREA Academia" for excellence in research funded by the Generalitat de Catalunya. B. G. M. is thankful to CONACYT for the financial support through a postgraduate scholarship (328467 CVU 621314). C.M. and E.A.P. thank the Belgian National Fund for Scientific Research for their research associate and senior research associate positions, respectively. Authors are thanked to Mr. Jordi Sans for his help in XPS measurements.

Appendix A. Supplementary data

Supplementary data to this article can be found online at https://doi.org/10.1016/j.memsci.2020.117931.

References

[1] D.M. Vriezema, M. Comellas Aragonès, J.A.A.W. Elemans, J.J.L.M. Cornelissen, A. E. Rowan, R.J.M. Nolte, Self-assembled nanoreactors, Chem. Rev. 105 (2005) 1445–1490, https://doi.org/10.1021/cr0300688.
[2] J.R. Werber, C.O. Osuji, M. Elimelech, Materials for next-generation desalination and water purification membranes, Nat Rev Mater 1 (2016) 16018, https://doi.org/10.1038/natrevmats.2016.18.
[3] A. Puiggalí-Jou, L.J. del Valle, C. Alemán, Biomimetic hybrid membranes: incorporation of transport proteins/peptides into polymer supports, Soft Matter 15 (2019) 2722–2736, https://doi.org/10.1039/C8SM02513D.
[4] Y.-R. Kim, S. Jung, H. Ryu, Y.-E. Yoo, S.M. Kim, T.-J. Jeon, Synthetic biomimetic membranes and their sensor applications, Sensors 12 (2012) 9530–9550, https://doi.org/10.3390/s120709530.
[5] S. Mura, J. Nicolas, P. Couvreur, Stimuli-responsive nanocarriers for drug delivery, Nat. Mater. 12 (2013) 991–1003, https://doi.org/10.1038/nmat3776.
[6] R. Koebnik, K.P. Locher, P. Van Gelder, Structure and function of bacterial outer membrane proteins: barrels in a nutshell, Mol. Microbiol. 37 (2000) 239–253, https://doi.org/10.1046/j.1365-2958.2000.01983.x.
[7] S. Galdiero, A. Falanga, M. Cantisani, R. Tarallo, M. Elena Della Pepa, V. D'Oriano, M. Galdiero, M.E. Della Pepa, V. D'Oriano, M. Galdiero, Microbe-host interactions: Structure and role of gram-negative bacterial porins, Curr. Protein Pept. Sci. 13 (2012) 843–854, https://doi.org/10.2174/138920312804871120.
[8] J.C. Ahumada, C. Alemán, J. Soto-Delgado, J. Torras, Ion-ion repulsions and charge-shielding effects dominate the permeation mechanism through the OmpF porin channel, J. Phys. Chem. B 123 (2019) 86–94, https://doi.org/10.1021/acs.jpcb.8b09549.
[9] J.H. Kleinschmidt, Folding and stability of monomeric β-barrel membrane proteins, in: Protein-Lipid Interactions, Weinheim, FRG, Wiley-VCH Verlag GmbH & Co. KGaA, 2006, pp. 27–56.
[10] M. Lopes-Rodrigues, A. Puiggalí-Jou, D. Martí-Balleste, L.J. del Valle, C. Michaux, E.A. Perpetè, C. Alemán, Thermomechanical response of a representative porin for biomimetics, ACS Omega 3 (2018) 7856–7867, https://doi.org/10.1021/acsomega.8b00463.
[11] M.M. Pérez-Madrigal, L.J. del Valle, E. Armelin, C. Michaux, G. Roussel, E. A. Perpète, C. Alemán C, Polypyrrole-supported membrane proteins for bio-inspired ion channels, ACS Appl. Mater. Interfaces 7 (2015) 1632–1643, https://doi.org/10.1021/am507142f.
[12] A. Puiggalí-Jou, M.M. Pérez-Madrigal, L.J. del Valle, E. Armelin, M.T. Casas, C. Michaux, E.A. Perpète, F. Estrany, C. Alemán, Confinement of a β-barrel protein in nanoperforated free-standing nanomembranes for ion transport, Nanoscale 8 (2016) 16922–16935, https://doi.org/10.1039/c6nr04948f.
[13] A. Puiggalí-Jou, J. Pawlowski, L.J. Valle, E.A. Perpète, S. Sek, C. Alemán, Properties of Omp2a-based supported lipid bilayers: Comparison with polymeric bioinspired membranes, ACS Omega 3 (2018) 9003–9019, https://doi.org/10.1021/acsomega.8b00913.
[14] O. Bubnova, Z.U. Khan, H. Wang, S. Braun, D.R. Evans, M. Fabretto, P. Hojati-Talemi, D. Dagnelund, J.B. Arlin, Y.H. Geerts, S. Desbief, D.W. Breiby, J. W. Andreasen, R. Lazzaroni, W.M. Chen, I. Zozoulenko, M. Fahlman, P.J. Murphy, M. Berggren, X. Crispin, Semi-metallic polymers, Nat. Mater. 13 (2014) 190–194, https://doi.org/10.1038/nmat3824.
[15] L.V. Kayser, D.J. Lipomi, Stretchable conductive polymers and composites based on PEDOT and PEDOT:PSS, Adv. Mater. 31 (2019) 1806133, https://doi.org/10.1002/adma.201806133.
[16] L.D. Sappia, E. Piccinini, W. Marmisolle, N. Santilli, E. Maza, S. Moya, F. Battaglini, R.E. Madrid, O. Azzaroni, Integration of biorecognition elements on PEDOT platforms through supramolecular interactions, Adv. Mater. Interf. 17 (2017) 1700502, https://doi.org/10.1002/admi.201700502.
[17] L.B. Groenendaal, F. Jonas, D. Freitag, H. Pielartzik, J.R. Reynolds, Poly(3,4-ethylenedioxythiophene) and its derivatives: Past, present, and future, Adv. Mater. 12 (2000) 481–494, https://doi.org/10.1002/(SICI)1521-4095(200004)12:7<481::AID-ADMA481>3.0.CO;2-C.
[18] D. Aradilla, F. Estrany, C. Alemán, Symmetric supercapacitors based on multilayers of conducting polymers, J. Phys. Chem. C 115 (2011) 8430–8438, https://doi.org/10.1021/jp201108c.
[19] B.W. Hoogenboom, K. Suda, A. Engel, D. Fotiadis, The supramolecular assemblies of voltage-dependent anion channels in the native membrane, J. Mol. Biol. 370 (2007) 246–255, https://doi.org/10.1016/j.jmb.2007.04.073.
[20] K. Zeth, Structure and evolution of mitochondrial outer membrane proteins of β-barrel topology, Biochim. Biophys. Acta Bioenerg. 1797 (2010) 1292–1299, https://doi.org/10.1016/j.bbabio.2010.04.019.
[21] T. Salinas, S. El Farouk-Ameqrane, E. Ubrig, C. Sauter, A.-M.M. Duchêne, L. Maréchal-Drouard, Molecular basis for the differential interaction of plant mitochondrial VDAC proteins with tRNAs, Nucleic Acids Res. 42 (2014) 9937–9948, https://doi.org/10.1093/nar/gku728.
[22] S. Hiller, R.G. Garces, T.J. Malia, V.Y. Orekhov, M. Colombini, G. Wagner, Solution structure of the integral human membrane protein VDAC-1 in detergent micelles, Science 321 (2008) 1206–1210, https://doi.org/10.1126/science.1161302.
[23] M. Colombini, The VDAC channel: Molecular basis for selectivity, Biochim. Biophys. Acta Mol. Cell Res. 1863 (2016) 2498–2502, https://doi.org/10.1016/j.bbamcr.2016.01.019.
[24] B.G. Molina, S. Cuesta, H. Besharatloo, J.J. Roa, E. Armelin, C. Alemán, Free-standing faradaic motors based on biocompatible nanoperforated poly(lactic acid) layers and electropolymerized poly(3,4-ethylenedioxythiophene), ACS Appl. Mater. Interfaces 11 (2019) 29427–29435, https://doi.org/10.1021/acsami.9b08678.
[25] B. Molina, S. Cuesta, A. Puiggalí-Jou, L.J. del Valle, E. Armelin, C. Alemán, Perforated polyester nanomembranes as templates of electroactive and robust free-standing films, Eur. Polym. J. 114 (2019) 213–222, https://doi.org/10.1016/j.eurpolymj.2019.02.038.
[26] A. Puiggalí-Jou, J. Medina, L.J. del Valle, C. Alemán, Nanoperforations in poly (lactic acid) free-standing nanomembranes to promote interactions with cell filopodia, Eur. Polym. J. 75 (2016) 552–564, https://doi.org/10.1016/j.eurpolymj.2016.01.019.
[27] G. Zotti, S. Zecchin, G. Schiavon, F. Louwet, L. Groenendaal, X. Crispin, W. Osikowicz, W. Salaneck, M. Fahlman, Electrochemical and XPS studies toward the role of monomeric and polymeric sulfonate counterions in the synthesis, composition, and properties of poly(3,4-ethylenedioxythiophene), Macromolecules 36 (2003) 3337–3344, https://doi.org/10.1021/ma021715k.
[28] K. Rechendorff, M.B. Hovgaard, M. Foss, V.P. Zhdanov, Besenbacher, Enhancement of protein adsorption induced by surface roughness, Langmuir 22 (2006) 10885–10888, https://doi.org/10.1021/la0621923.
[29] V.K. Garg, H. Avashthi, A. Tiwari, P.A. Jain, P.W. Ramkete, A.M. Kayastha, V. K. Singh, MFPPI - Multi FASTA ProtParam interface, Bioinformation 12 (2016) 74–77, https://doi.org/10.6026/97320630012074.
[30] S. Maione, A.M. Gil, G. Fabregat, L.J. del Valle, J. Triguero, A. Laurent, D. Jacquemin, F. Estrany, A.I. Jiménez, D. Zanuy, C. Cativiela, C. Alemán,

Electroactive polymer–peptide conjugates for adhesive biointerfaces, Biomater. Sci. 3 (2015) 1395–1405, https://doi.org/10.1039/C5BM00160A.
[31] S. Maione, G. Fabregat, L.J. del Valle, A.-D. Bendrea, L. Cianga, I. Cianga, F. Estrany, C. Alemán, Effect of the graft ratio on the properties of polythiophene-g-poly(ethylene glycol), J. Polym. Sci., Part B: Polym. Phys. 53 (2015) 239–252, https://doi.org/10.1002/polb.23617.
[32] H.J. Perera, H. Mortazavian, F.D. Blum, Surface properties of silane-treated diatomaceous earth coatings: effect of alkyl chain length, Langmuir 33 (2017) 2799–2809, https://doi.org/10.1021/acs.langmuir.7b00015.
[33] A.A. Moya, Identification of characteristic time constants in the initial dynamic response, J. Power Sources 397 (2018) 124–133, https://doi.org/10.1016/j.jpowsour.2018.07.015.
[34] A.A. Moya, Electrochemical impedance of ion-exchange membranes with interfacial charge transfer resistances, J. Phys. Chem. C 120 (2016) 6543–6552, https://doi.org/10.1021/acs.jpcc.5b12087.
[35] P. Córdoba-Torres, Relationship between constant-phase element (CPE) parameters and physical properties of films with a distributed resistivity, Electrochim. Acta 225 (2017) 592–604, https://doi.org/10.1016/j.electacta.2016.12.087.
[36] J. Poater, J. Casanovas, M. Solà, C. Alemán, Examining the planarity of poly(3,4-ethylenedioxythiophene): Consideration of self-rigidification, electronic, and geometric effects, J. Phys. Chem. 114 (2010) 1023–1028, https://doi.org/10.1021/jp908764s.
[37] T. Rostovtseva, M. Colombini, VDAC channels mediate and gate the flow of ATP: implications for the regulation of mitochondrial function, Biophys. J. 72 (1997) 1954–1962, https://doi.org/10.1016/S0006-3495(97)78841-6.
[38] G. Smith, M.S. Sansom, Effective diffusion coefficients of K^+ and Cl^- ions in ion channel models, Biophys. Chem. 79 (1999) 129–151, https://doi.org/10.1016/S0301-4622(99)00052-6.
[39] A.K.S. Camara, Y. Zhou, P.-C. Wen, E. Tajkhorshid, W.-M. Kwok, Mitochondrial VDAC1: A key gatekeeper as potential therapeutic target, Front. Physiol. 8 (2017) 460, https://doi.org/10.3389/fphys.2017.00460.
[40] L. Shao, K.W. Kinnally, C.A. Mannella, Circular dichroism studies of the mitochondrial channel, VDAC, from *Neurospora crassa*, Biophys. J. 71 (1996) 778, https://doi.org/10.1016/S0006-3495(96)79277-9.
[41] M. Lopes-Rodrigues, A. Puiggalí-Jou, D. Martí-Balleste, L.J. del Valle, C. Michaux, E.A. Perpète, C. Alemán, Thermomechanical response of a representative porin for biomimetics, ACS Omega 3 (2018) 7856, https://doi.org/10.1021/acsomega.8b00463.
[42] G.L. Rosano, E.A. Ceccarelli, Recombinant protein expression in Escherichia coli: advances and challenges, Front. Microbiol. 5 (2014) 172, https://doi.org/10.3389/fmicb.2014.00172.
[43] S. Schlegel, A. Hjelm, T. Baumgarten, D. Vikstrom, J.W. de Gier, Bacterial-based membrane protein production, Biochim. Biophys. Acta 1843 (2014) 1739, https://doi.org/10.1016/j.bbamcr.2013.10.023.
[44] M. Fernández de Labastida, A. Yaroshchuk, Transient membrane potential after concentration step: A new method for advanced characterization of ion-exchange membranes, J. Membr. Sci. 585 (2019) 271, https://doi.org/10.1016/j.memsci.2019.05.012.
[45] N. Pismenskaia, P. Sistat, P. Huguet, V. Nikonenko, G. Pourcelly, Chronopotentiometry applied to the study of ion transfer through anion exchange membranes, J. Membr. Sci. 228 (2004) 65, https://doi.org/10.1016/j.memsci.2003.09.012.